Available online at www.sciencedirect.com
ScienceDirect
Journal of Power Sources 159 (2006) 869–877
JOURNAL OF POWER SOURCES
www.elsevier.com/locate/jpowsour

Preparation and characterization of supported Pt–Ru catalysts with a high Ru content

Luciano dos Santos, Flavio Colmati, Ernesto R. Gonzalez *

Instituto de Química de São Carlos, USP, C.P. 780, 13560-970 São Carlos, SP, Brazil

Received 17 November 2005; accepted 15 December 2005
Available online 23 February 2006

Abstract

Pt–Ru nanoparticles supported on high surface area carbon were synthesized by reduction of the precursors with sodium formate, a modification of the reduction method with formic acid developed in this laboratory, which allows the incorporation of higher amounts of Ru. The catalysts were characterized by EDX and XRD. Electrochemical experiments involved cyclic voltammetry, linear sweep voltammetry and current–potential curves for the oxidation of hydrogen and carbon monoxide using an ultrathin layer rotating disc electrode. Levich and Tafel plots were used to examine the mechanism of the reactions. The results were compared with those obtained using a commercial Pt–Ru catalyst.

Keywords: Supported catalysts; Pt–Ru; Ultrathin layer RDE; H_2 oxidation; CO oxidation

1. Introduction

Fuel cells are electrochemical energy converters that can operate with high efficiencies without contaminating the environment. They operate by oxidizing a fuel at the anode and reducing atmospheric oxygen at the cathode, and the electrodes are separated by an ion conducting medium [1]. Low temperature fuel cells (<200 °C) require the use of efficient electrocatalysts in order to accelerate the rate of the reactions and among the different types [2], the proton exchange membrane fuel cells (PEMFC) are the most promising for vehicles and portable equipment because they are characterized by high power densities. These fuel cells can oxidize hydrogen or low molecular weight alcohols [3].

PEMFCs operating with pure hydrogen can deliver high power densities. However, the hydrogen fuel is expensive and presents technological problems of production, storage and distribution. Additionally, the cheapest way of producing hydrogen is the catalytic reforming of other fuels, which produces a hydrogen contaminated with unacceptable amounts of carbon monoxide. Because of this, intensive research is devoted to the direct use of methanol as a fuel (direct methanol fuel cell, DMFC). Methanol is much easier to handle, can be produced from renewable sources and the DMFC has a theoretical cell potential of 1.21 V at room temperature, very near the value of 1.23 V of the PEMFC. The two main problems of the DMFC are the slow kinetics of the electro-oxidation of methanol and the fact that methanol can migrate across the proton exchange membrane toward the cathode compartment where it can be oxidized, reducing the efficiency of the cell. Even with these restrictions, DMFCs are getting near the goal of delivering a power density of 0.3 W cm^{-2}.

The most widely used catalysts in low temperature fuel cells are platinum and platinum-based alloys. However, the oxygen reduction reaction and the oxidation of methanol are slow on those catalysts and efforts are being made to improve the kinetics of the reactions. The main problem with anode catalysts based on Pt is the strong adsorption of CO on Pt. As stated above, CO contaminates industrially produced hydrogen and it is also formed as an intermediate in the electro-oxidation of methanol [4]. Because of this, the oxidation of CO on platinum-based materials has been studied for many decades [5]. The effect of the presence of CO is such that 5 ppm can reduce in 50% the efficiency of a fuel cell operating with a fast reaction like the oxidation of hydrogen on platinum [6] (the exchange current density is 3.16 mA cm^{-2} at pH 0.5).

One of the usual ways of improving the tolerance of platinum to CO is to alloy it with transition metals. The most widely

* Corresponding author. Tel.: +55 16 3373 9899; fax: +55 16 3373 9952.
E-mail address: ernesto@iqsc.usp.br (E.R. Gonzalez).

0378-7753/$ – see front matter © 2006 Elsevier B.V. All rights reserved.
doi:10.1016/j.jpowsour.2005.12.086

investigated material of this type is the Pt–Ru alloy [7–13] and to a lesser extent Pt–Sn [12], Pt–Re [14], Pt–Mo [15,16] and also some ternary materials, like Pt–Ru–Sn [17]. One of the problems with these alloys is the instability under continuous operation.

Igarashi et al. [18], classified the transition metals into three groups with Ru belonging to the group of the most active materials. More specifically, Hou et al. [16] showed that Pt–Ru/C with a metal atomic composition 50:50 and 20 wt.% on carbon presents the highest activity for the oxidation of CO. This has been attributed to the formation of hydrated oxides on the Ru, which facilitate the oxidation of CO [17,19]. Several binary alloys operate through a bifunctional mechanism. Oxygenated species nucleate on the second metal, at lower potentials than on platinum, and promote the oxidation of CO adsorbed on Pt sites, leaving free sites for the anodic oxidation of the fuel [20,21].

It is well known that CO adsorbs on platinum in three main configurations: the linear form, involving one platinum atom per CO molecule, the bridge form, involving two platinum atoms per CO molecule and the three-fold form, involving three platinum atoms per CO molecule [22].

Pt–Ru catalysts were synthesized previously in this laboratory by reduction of the precursors with formic acid [23], but this resulted in materials with relatively low Ru contents (up to 25 at.%). In this work, the method was modified in order to obtain Pt–Ru catalysts with higher Ru contents. These materials were characterized by physical methods and it was considered of interest to characterize them electrochemically with respect to the hydrogen and carbon monoxide oxidation reactions.

2. Experimental

2.1. Preparation of the Pt–Ru/C catalysts

A method to prepare Pt/C [23] and binary catalysts like Pt–Sn/C [24] and Pt–Co/C [25] through the reduction of precursors with formic acid was developed in this laboratory. However, when used to synthesize Pt–Ru/C it was not possible to prepare materials with Ru content greater than 25 at.%. One possible explanation for this limitation is that formic acid has a dissociation constant of 1.8×10^{-5}, so there is a low concentration of the reducing agent, the formate anion. Furthermore, the value of the reduction potential and the oxidation state of any element depends on the pH according to the Nernst equation [26]:

$$E_{\text{red}} = E_0^{\circ} + \frac{2.3RT}{nF} \log \frac{(a_{\text{A}})^{\text{a}}}{(a_{\text{B}})^{\text{b}}} - \frac{2.3RT}{F}\frac{m}{n}\text{pH} \quad (1)$$

where a is the activity of the reactants, E_0° is the standard potential and m, n, a and b are the stoichiometric coefficients of a general reaction as $a\text{A} + m\text{H}^+ + n\text{e}^- \rightarrow b\text{B} + c\text{H}_2\text{O}$, and the other parameters have the usual meaning.

For the present case of reduction of Ru^{3+} (from the precursor $RuCl_3$) to metallic Ru, at 25 °C and in aqueous solution, the dependence of the reduction potential on the pH is given by [26]:

$$E_{\text{red}} = -0.738 + 0.0591\,\text{pH} \quad (2)$$

and the dependence of the oxidation potential on the pH for the conversion of formic acid to carbon dioxide, under the same experimental conditions, is given by [27]:

$$E_{\text{ox}} = 0.249 + 0.0591\,\text{pH} \quad (3)$$

Thus, in this work, the pH of the formic acid solutions was increased to 14 by the addition of sodium hydroxide, converting all the undissociated formic acid into formate. This solution, in a constant-temperature bath at 80 °C, was used to impregnate carbon powder (Vulcan XC-72, Cabot, 240 $m^2\,g^{-1}$, thermically treated in a tubular furnace at 850 °C, in an Argon Atmosphere for 5 h). Then, solutions of $RuCl_3{\cdot}xH_2O$ and $H_2PtCl_6{\cdot}6H_2O$ in the chosen proportions were slowly added to the formate-impregnated carbon and the dispersion was maintained under stirring until complete reduction of the metals. The resulting supported catalyst was then filtered and washed.

Syntheses were done at different pH's. The precursors concentration ratio was difficult to adjust quantitatively due to unknown water contents in the salts but roughly the amounts used should produce theoretically a 50:50 atomic ratio of the metals. Furthermore, the same amounts of precursors were used for all syntheses. It was observed that at pH 10 the reduction of Ru ions was not complete. By rising the pH to 14 then the reduction of Ru ions was indeed complete. For the sake of simplicity this preparation procedure will be called sodium formate method (SFM).

After filtering, part of each catalyst was submitted to a thermal treatment (TT) at 300 °C for 1 h, in a reducing hydrogen atmosphere. The TT was designed to prevent a segregation of Ru and to promote a possible alloy formation between the metals.

2.2. Characterization of the catalysts

The Pt and Ru contents of the catalysts were determined by EDX using a Zeiss Digital Scanning Electron Microscope DSM 960 with a microanalyser Link Analytical QX 2000 with an electron beam of 63 keV.

The average metal particle size and the lattice parameter were determined by XRD using an universal diffractometer Carl-Zeiss-Jena URD-6 operating with Cu Kα radiation ($\lambda = 0.15406$ nm) generated with 40 kV and 20 mA. The scanning was done at 3° min^{-1} for values of 2θ between 30° and 100°.

2.3. Preparation of the working electrode

The ultrathin layer working electrode was prepared by applying 30 μL from a suspension of the catalysts, dispersed ultrasonically in ultrapure water, on a glassy carbon disk (0.374 cm^2 geometrical surface area) embedded on a PTFE support [28]. In all cases the catalyst applied contained 28 μg Pt cm^{-2}. A small drop of 5% Nafion® solution was applied on the catalyst to fix the powder and ensure ionic conductivity. Then, the electrode was dried under vacuum and transferred to the electrochemical cell covered with a drop of ultrapure water to protect the

catalytic surface and immersed under potential control at 0.05 V in a nitrogen-saturated 0.5 mol L^{-1} H_2SO_4 electrolyte. Using this method, the catalyst layer has a thickness of only 0.5 μm, which according to Schmidt et al. [28] should not introduce mass transport effects.

2.4. Electrochemical studies

The electrochemical studies were carried out in a three-electrode cell using a reversible hydrogen electrode as reference and a platinum grid electrode as secondary electrodes. The cell was controlled with an Autolab potentiostat PGSTAT 30. In the RDE experiments the working electrode was rotated in the range 400–2500 rpm using a PINE Instruments AFCPRB rotator.

Cyclic voltammetry (CV) experiments were carried out in a 0.5 mol L^{-1} H_2SO_4 electrolyte, in the absence of oxygen, at a scan rate of 20 mV s^{-1} to evaluate the state of the surface [29–31].

Linear sweep voltammetry (LSV) experiments were used to study the oxidation of CO. Maintaining the electrode at 0.05 V, the solution was saturated with CO by bubbling the gas for at least 10 min for complete adsorption. The excess CO was eliminated by bubbling nitrogen and then the LSV was recorded.

Steady-state current–potential curves were recorded after saturating the electrolyte with H_2 or CO under potential control at 0.05 and 0.60 V, respectively, and the reagent gas was passed through the solution for the duration of the experiment.

3. Results and discussion

3.1. Characterization of the catalysts

The EDX analyses showed that with the same concentration of the precursors the Pt:Ru atomic ratio of the catalyst synthesized at pH 10 was 65:35, while at pH 14 the ratio was 40:60. Fig. 1 shows the EDX spectrum for this last material after the thermal treatment. The EDX spectrum shows the presence of fluorine, from the PTFE used in the preparation of the sample and sodium, probably coming from the NaOH used to rise the pH. One possible explanation for the lower Ru content of the catalyst synthesized at the lower pH is the formation of Ru(III) complexes with formic acid that have been described in the literature [32]. So it is plausible that, apart from the beneficial effect on the reduction potential, the formation of complexes is inhibited at higher pH's. The metal content of the catalysts was 23.6 wt.% for $Pt_{65}Ru_{35}$/C and 25.8 wt.% for $Pt_{40}Ru_{60}$/C.

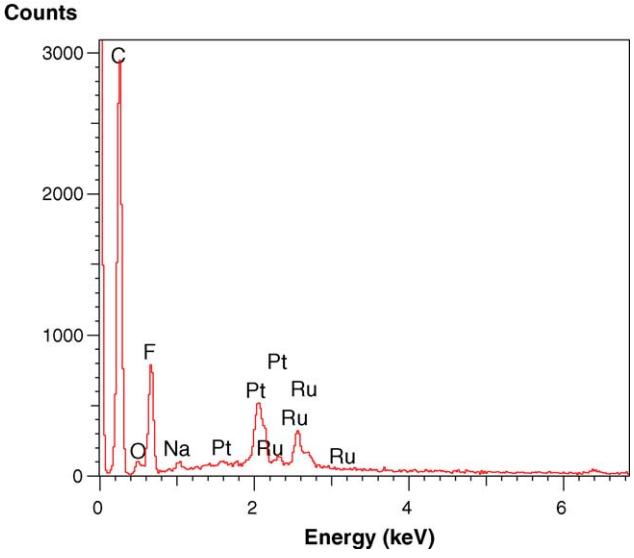

Fig. 1. EDX spectrum of $Pt_{40}Ru_{60}$/C SFM TT.

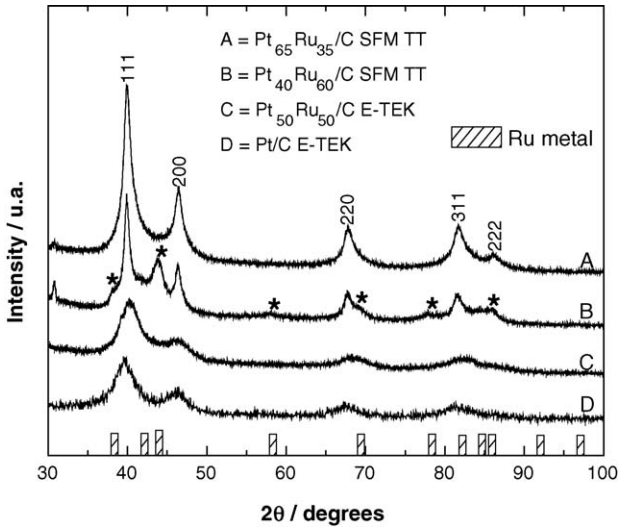

Fig. 2. XRD diffractograms of the Pt–Ru/C SFM TT materials and of Pt–Ru/C and Pt/C E-TEK. (⋆) hexagonal structure refraction peaks of metalic Ru. ( ) Joint Committee on Powder Diffraction Data (JCPDS) card 6-633.

Fig. 2 shows the X-ray diffractograms for the two catalysts synthesized here and submitted to thermal treatment and also for the materials Pt/C and $Pt_{50}Ru_{50}$/C E-TEK, used for comparison. Using the peak (2 2 0) of the fcc structure, which is not influenced by the broad peak of the carbon support, the particle sizes were estimated using Scherrer's equation [33] and the lattice parameters estimated using Bragg's law [34]. Table 1 presents the results for all the materials and also the lattice parameters of pure Pt and Ru for reference. The results in Table 1 show that the materials submitted to thermal treatment have a larger particle size indicating that the thermal treatment induces sintering and coalescence of the particles. They also show smaller values of

Table 1
Mean particle sizes, lattice parameters and electroactive areas for the different supported catalysts

Catalyst	Mean particle size (nm)	Lattice parameter (Å)	Electroactive area (m^2 g^{-1})
$Pt_{65}Ru_{35}$/C SFM	5.1	3.9079	–
$Pt_{65}Ru_{35}$/C SFM TT	5.7	3.9005	87.6
$Pt_{40}Ru_{60}$/C SFM	4.6	3.9086	–
$Pt_{40}Ru_{60}$/C SFM TT	5.2	3.8969	62.8
$Pt_{50}Ru_{50}$/C E-TEK [35]	3.2	3.888	129.6
Pt/C E-TEK [35]	2.9	3.915	–
Pt metal [35]	–	3.9239	–
Ru metal [35]	–	2.7058	–

the lattice parameter, which indicates a contraction of the lattice due to the increase in the amount of Ru in the alloyed state favored by the high temperature. The results in Table 1 show that the $Pt_{40}Ru_{60}$ material synthesized here has a value larger than that of the $Pt_{50}Ru_{50}$ E-TEK. If it is assumed that in this last material the two metals are in the alloyed state, it must be concluded that in the $Pt_{40}Ru_{60}$ catalyst part of the Ru is present either as metal or in the form of oxides. The diffractogram of this material in Fig. 2 shows clearly the presence of hexagonal Ru peaks (JCPDS card 6-663), and the presence of oxides cannot be discarded because they are amorphous and do not show in the diffractogram.

Pourbaix and Franklin [26] concluded that $RuCl_3$ (used here as precursor of Ru) is converted into $Ru(OH)_3$ by addition of alkali in the solution, and this species is stable in water and aqueous solutions of all pH's when free from oxidizing or reducing agents. In the presence of reducing agents, $Ru(OH)_3$ can be easily reduced to elementary ruthenium, as deduced from Eq. (2). In order to have a quantitative estimative of conditions during the synthesis, the reaction potential for the reduction of Ru^{3+} to metallic Ru and for the oxidation of $HCOO^-$ to CO_2 were calculated using the concentrations of the precursors and pH 14 into Eq. (1) for the following reactions:

$$2\,Ru(OH)_3 + 6\,H^+ + 6\,e^- \leftrightarrows 2Ru + 6\,H_2O \quad E = 0.09\,V$$

$$3\,HCOOH \leftrightarrows 3\,CO_2 + 6\,H^+ + 6\,e^- \quad E = 1.08\,V$$

$$2\,Ru(OH)_3 + 3\,HCOOH \leftrightarrows 2\,Ru + 3\,CO_2 + 6\,H_2O \quad E = 1.17\,V$$

The resulting value of 1.17 V is positive enough to favor the spontaneous reaction. On the other hand, at low pH's the value of potential of the overall reaction may reach negative values, which does not favor the reduction of Ru^{3+}. So, considering the conditions of preparation of the catalysts and the presence of the hexagonal Ru peaks in the diffractogram, it is plausible to conclude that part of the Ru in the catalyst is present in the metallic form.

3.2. Electrochemical experiments

Fig. 3 shows the cyclic voltammograms (CV) of the catalysts prepared with the SFM and submitted to thermal treatment, in comparison with Pt–Ru E-TEK. The upper limit of the CVs was 0.8 V to prevent any Ru dissolution. The profiles of the voltammograms in the double layer region are similar for the three materials and the currents are larger for $Pt_{40}Ru_{60}$ because of the formation of oxygenated species on Ru. It is interesting to note that the hydrogen region is more suppressed on the $Pt_{50}Ru_{50}$/C E-TEK material, as a consequence of a higher degree of alloy formation than in $Pt_{40}Ru_{60}$/C SFM TT. The oxidation of hydrogen would not be favored on an alloy because the exchange current density on Ru ($\cong$0.003 A cm^{-2}) is much smaller than that on Pt ($\cong$0.3 A cm^{-2}) [9].

Fig. 4 shows the linear sweep voltammetries for the oxidation of CO, previously adsorbed at 0.05 V. It is widely accepted that

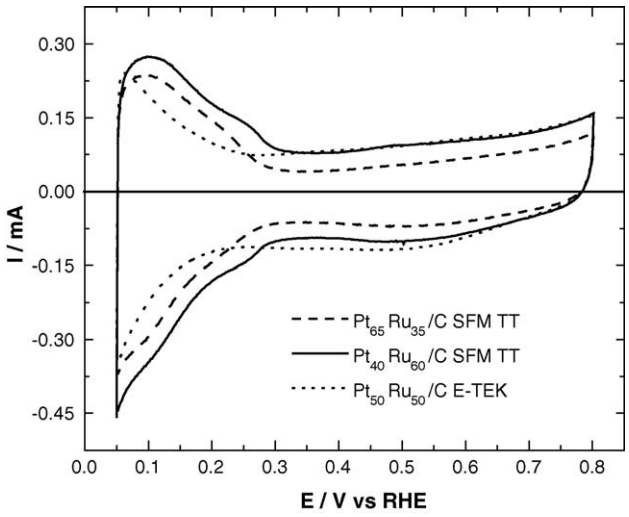

Fig. 3. Cyclic voltammograms of some of the catalysts, obtained with an ultrathin layer electrode at 25 °C in 0.5 mol L^{-1} H_2SO_4 solution.

on Pt–Ru the oxidation of CO to CO_2 occurs mainly through a Langmuir–Hinshelwood mechanism [36]. On Pt–Ru the oxidation starts at lower potentials than on Pt because the necessary oxygenated species are formed at lower potentials on Ru. This is evidenced here by the fact that on $Pt_{40}Ru_{60}$ CO is oxidized at lower potentials than on the other materials. Additionally, it seems that thermal treatments increase the CO tolerance of Pt–Ru catalysts [37,38]. Fig. 4 also shows the presence of a small second oxidation peak for the $Pt_{40}Ru_{60}$ material. This second peak is near the potential value at which CO is oxidized on pure Pt and it may indicate the presence of segregated Pt metal on the material.

The charge corresponding to the oxidation of CO, in the potential interval between 0.40 and 0.80 V, was used to calculate the electroactive area of the thermally treated SFM catalysts

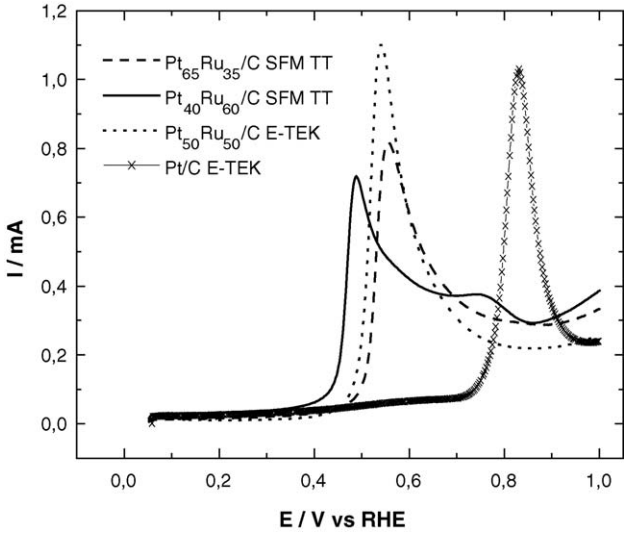

Fig. 4. Linear sweep voltammograms for the oxidation of CO_{ads} on some of the catalysts, obtained with an ultrathin layer electrode at 25 °C in 0.5 mol L^{-1} H_2SO_4 solution. CO was previously adsorbed at 0.05 V (vs. RHE).

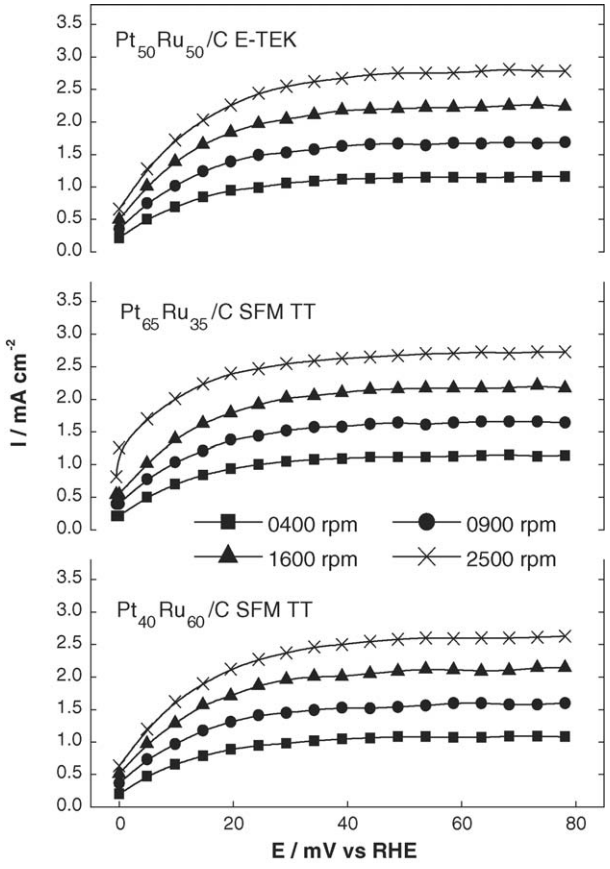

Fig. 5. Steady-state current–potential plots for the oxidation of hydrogen at different rotation speeds, at 25 °C in 0.5 mol L^{-1} H_2SO_4 solution.

and the E-TEK catalyst, assuming a charge of 420 μC cm^{-2} for the oxidation of a monolayer of CO. The results, normalized by the Pt load, are presented in Table 1. It is interesting to note that the ratio between the electroactive areas of $Pt_{65}Ru_{35}$ and $Pt_{50}Ru_{50}$ E-TEK (0.7) correlates well with the inverse ratio of the corresponding particle sizes shown in Table 1 (0.6). The same relationship was observed for $Pt_{40}Ru_{60}$ and $Pt_{50}Ru_{50}$ E-TEK, where the ratio between the electroactive areas is 0.5 and the inverse ratio of the corresponding particle sizes is 0.6. The differences can easily be rationalized in terms of the uncertainties in the values.

Fig. 5 shows the steady-state current–potential curves for the oxidation of hydrogen on the different materials and at different rotation speeds. At low potentials the current is controlled by the activation overpotential. As the potential increases, mass transport starts to influence the current until a limiting current, favored by the low solubility of hydrogen (7.14×10^{-3} mol L^{-1} [8]), is reached. Fig. 5 shows that the limiting current increases with the rotation speed and for a purely diffusion controlled system the relationship is given by the well known Levich equation:

$$i_L = 0.62nFAD^{2/3}\nu^{-1/6}C\omega^{1/2} \quad (4)$$

where A is the geometric area of the electrode, D the diffusion coefficient of the reacting species, ν the kinematic viscosity, and

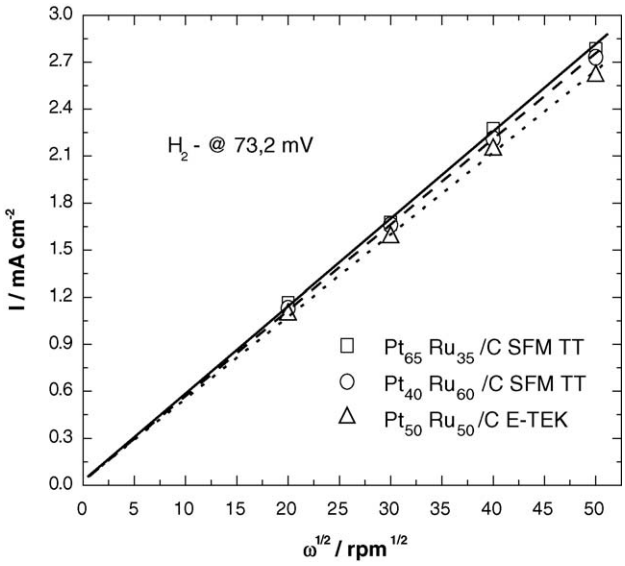

Fig. 6. Levich diagrams for the oxidation of hydrogen on different catalysts, at 25 °C in 0.5 mol L^{-1} H_2SO_4 solution.

ω is the rotation speed and the other symbols have their usual meaning.

Fig. 6 presents the Levich plots for the oxidation of hydrogen, which confirm the predictions of Eq. (4), i.e., they are straight lines going through the origin. This allows to conclude that the Nafion® film on the catalyst does not interfere with the diffusion process. According to Schmidt et al. [28] this should be the case for Nafion® films thinner than 0.5 μm as those used in this work. The only parameter in Eq. (4) that may depend on the catalyst is the area A, but as can be observed in Fig. 6, the ratio among the slopes of the curves has no mathematical relationship with the ratio among the electroactive areas of the catalysts, indicating that the limiting current density of the hydrogen oxidation reaction depends only on the geometric area of the electrode. This is expected when the thickness of the hydrodynamic layer is larger than the rugosity of the surface.

Fig. 7 shows the steady-state current–potential curves for the oxidation of CO in a saturated solution of this reactant. Here, the oxidation reaction requires much higher potentials than the oxidation of hydrogen. Also, because the reaction is much slower, the curves for the different materials and the different rotation speeds are not so well resolved as the curves in Fig. 5. Assuming that the main path for the oxidation of CO on Pt is a Langmuir–Hinshelwood mechanism, at high potentials and for the range of rotation speeds used here the reaction is also diffusion controlled and reaches a limiting current. As can be seen in Fig. 7, the potential for the onset of the reaction decreases as the amount of Ru in the catalysts increases, following the sequence $Pt_{40}Ru_{60} < Pt_{50}Ru_{50} < Pt_{65}Ru_{35}$. It can also be observed that for high rotation speeds (higher limiting currents) there is a slight decrease of the currents at high potentials. This may be a consequence of the reduction in available sites for CO oxidation as the surface is progressively covered with oxygenated species.

Fig. 8 shows the corresponding Levich plots for CO oxidation and although they are reasonably linear the straight lines do not

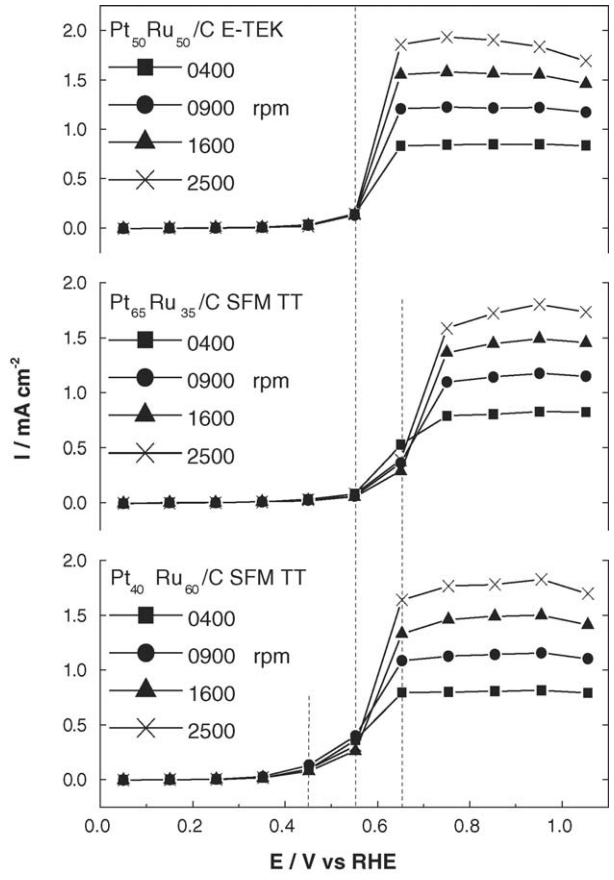

Fig. 7. Steady-state current–potential plots for the oxidation of CO at different rotation speeds, at 25 °C in 0.5 mol L^{-1} H_2SO_4 solution.

go through the origin as predicted by Eq. (4). Probably, this is due to the complexity of the mechanism of the reaction, which requires the diffusion and adsorption of CO on Pt sites and the formation of oxygenated species on Ru sites. It must be reminded that Eq. (4) is valid for species that upon reaching the electrode

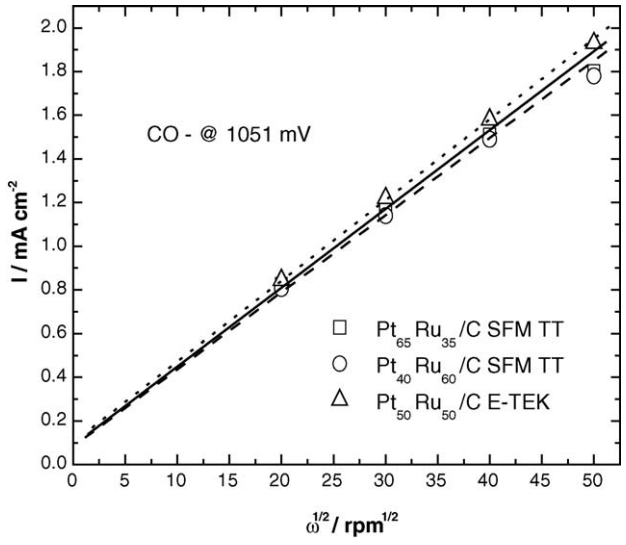

Fig. 8. Levich diagrams for the oxidation of CO on different catalysts, at 25 °C in 0.5 mol L^{-1} H_2SO_4 solution.

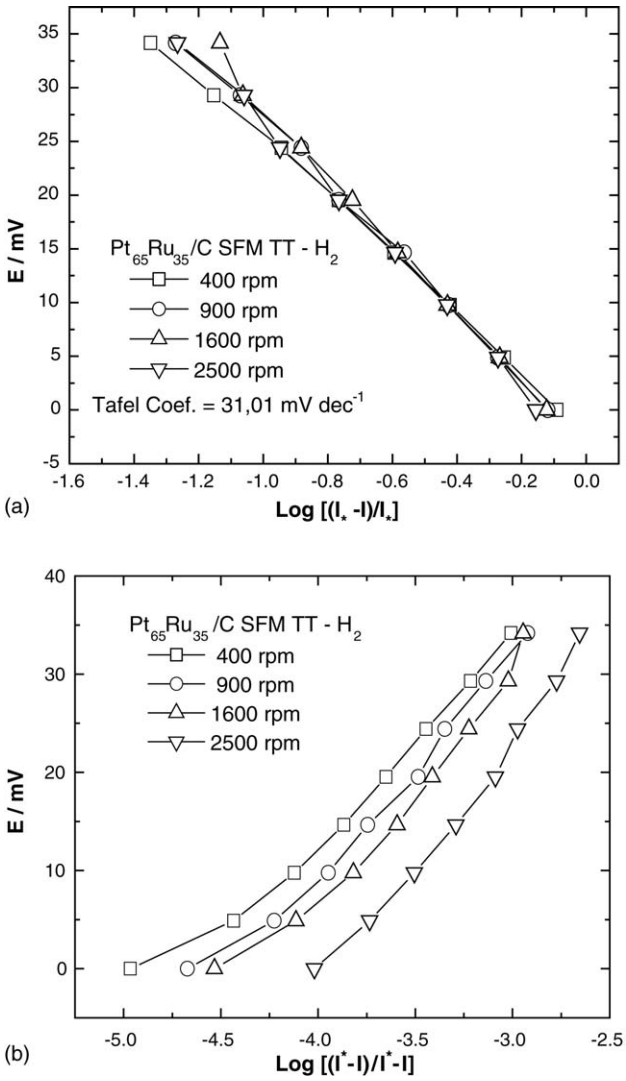

Fig. 9. (a) Mass transfer corrected Tafel plots assuming reversible kinetics for the oxidation of hydrogen on $Pt_{65}Ru_{35}$/C SFM TT, at 25 °C in 0.5 mol L^{-1} H_2SO_4 solution. (b) Mass transfer corrected Tafel plots assuming irreversible kinetics for the oxidation of hydrogen on $Pt_{65}Ru_{35}$/C SFM TT, at 25 °C in 0.5 mol L^{-1} H_2SO_4 solution.

surface by diffusion react immediately. Furthermore, Lima et al. [39] observed that for the oxygen reduction reaction in alkaline solution the straight lines of the Levich plots do not go through the origin. The authors attributed this to contributions to the current not included in the derivation of Eq. (4). Alternatively, deviations of the behavior predicted by Levich's equation may be due to the presence of turbulence in the electrode/electrolyte interface caused by the high roughness of the catalyst layer.

Using the steady-state current–potential values taken from Figs. 5 and 7 it is possible to construct mass transport corrected Tafel plots. But in order to construct these diagrams it is necessary to assume a priori whether the reaction is reversible or irreversible.

Fig. 9a and b shows the Tafel plots for the oxidation of hydrogen at different rotation speeds assuming that the reaction is reversible and irreversible, respectively. Only the plots

Table 2
Tafel slope for the hydrogen (HOR) and carbon monoxide (COOR) oxidation reactions and the corresponding charge transfer and symmetry coefficients

Catalyst	Tafel slope for reversible HOR (mV dec^{-1})	Tafel slope for irreversible COOR (mV dec^{-1})	Charge transfer coefficient (α) for COOR	Symmetry coefficient (β) for COOR
$Pt_{65}Ru_{35}$/C SFM TT	31.01	196.76	0.3003	0.537
$Pt_{40}Ru_{60}$/C SFM TT	30.14	136.69	0.4323	0.663
$Pt_{50}Ru_{50}$/C E-TEK	30.56	147.41	0.4008	0.600

for $Pt_{65}Ru_{35}$ are presented because they are representative of the results for the three materials. Because the current rises very fast only the values between 0 and 0.035 V could be used to construct the Tafel plots. The plots which assume a reversible kinetics (Fig. 9a) are independent of the rotation speed showing that, as expected, the reaction is fast. The values of the Tafel slopes are presented in Table 2 and for the three materials they are very near 30 mV dec^{-1}. From this value it may be concluded that the most probable mechanism for the reaction is the reversible direct discharge [40–42] for the three materials.

As expected, the results are markedly different for the oxidation of CO. Here, current values for potentials between 0.35 and 0.60 V were used to construct the Tafel plots of Fig. 10a and b for $Pt_{65}Ru_{35}$, which show that the reaction is irreversible. The values of the Tafel slopes presented in Table 2 are much higher than those observed for the oxidation of hydrogen and are consistent with the irreversibility of the reaction. Additionally, the high values of the Tafel slopes are not consistent with common kinetic pathways under Langmuir adsorption conditions. However, Flitt and Bockris [43] observed in their work about hydrogen evolution on ferrite with carbide inclusions that for coverages (θ) between 0.1 and 0.9 the form of the isotherm influences the relationship between current and potential. This means a different charge transfer coefficient (α) and hence a different slope from those where the hydrogen evolution reaction occurs on surfaces constituted of only one element (between 30 and 120 mV dec^{-1}). They observed a Tafel slope larger than 200 mV dec^{-1} in the presence of additives and a slope of about 180 mV dec^{-1} in the absence of additives and interpreted their results by applying Temkin isotherms, assuming that the hydrogen evolution in the interface between carbide and ferrite phases was the rate-determining step, with the mechanism being a coupled discharge-atomic recombination on the interfaces of the heterogeneous surface [43].

The values of the Tafel slope for CO oxidation seem to depend on the nature of the electrolyte. Arico et al. [44,45] measured values of 136 mV dec^{-1} in sulphuric and phosphotungstic acids. In Nafion®, Aberdam et al. [46] measured values as high as 320 mV dec^{-1}, but more recent works [36,47] found, by two different methods, 210 and 230 mV dec^{-1}. This may explain the discrepant values of the Tafel slopes presented in Table 2. Because of the procedure used to make the working electrode, the $Pt_{65}Ru_{35}$ catalyst may have been more covered by the Nafion® film, so the Tafel slope resulted higher than on the other two catalysts.

From the Tafel slopes presented here, it is possible to obtain kinetic parameters like the charge transfer and the symmetry coefficients (α and β, respectively), which for a complex charge transfer reaction are correlated to each other by

$$\alpha = \left(\frac{n-\gamma}{\nu}\right) - r\beta \tag{5}$$

for anodic reactions, where n is the number of electrons involved in the overall reaction, γ the number of electrons transferred

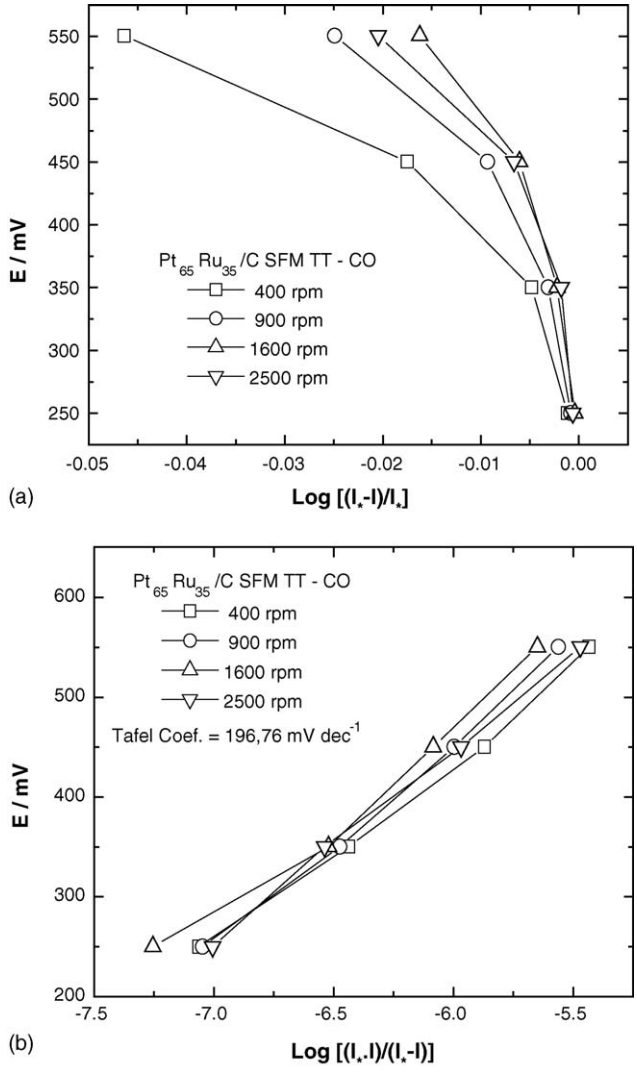

Fig. 10. (a) Mass transfer corrected Tafel plots assuming reversible kinetics for the oxidation of CO on $Pt_{65}Ru_{35}$/C SFM TT, at 25 °C in 0.5 mol L^{-1} H_2SO_4 solution. (b) Mass transfer corrected Tafel plots assuming irreversible kinetics for the oxidation of CO on $Pt_{65}Ru_{35}$/C SFM TT, at 25 °C in 0.5 mol L^{-1} H_2SO_4 solution.

before the rate-determining step, r the number of electrons involved in the rate-determining step (0 or 1) and ν is the stoichiometric number (the number of times the rate-determining step occurs for one act of the overall reaction) [48].

Eq. (5) shows that the charge transfer coefficient depends on the position of the maximum of the energy barrier of the transition state, i.e. the values of the symmetry coefficient, for the reaction between CO and OH species, which in turn may depend on the influence of the composition of the material on the electronic structure of the electrocatalysts. Assuming that the values of n, γ, ν and r are the same for all Pt–Ru compositions, the only parameter that may influence the value of α is the symmetry coefficient.

For the catalyst $Pt_{65}Ru_{35}$, the Tafel slope of 196.76 mV dec^{-1} is very close to ($2.3RT/0.3F$) at 25 °C, which corresponds to one electron being transferred in the rate-determining step for a reaction occurring on the interphase between two different materials, as exemplified by the work of Flitt and Bockris [43]. If it is considered that the rate-determining step is the reaction between CO and OH, it is possible to obtain a value of 0.7 for the symmetry coefficient, β, by using Eq. (5) with an experimental value of 0.3 for α and considering ν equal to 1 turn of OH adsorption on Ru sites for each turn of CO adsorption on Pt sites. The values for all the materials are presented in Table 2.

The values of Tafel slope observed for the studied materials are consistent with the reaction occurring in the interface between two different metals or sites (in the present case, CO on Pt sites and OH on Ru sites) as suggested in the work of Flitt and Bockris [43].

4. Conclusions

In the synthesis of Pt–Ru alloys via reduction of precursors, it was demonstrated in this work that an increase in the pH of the formic acid solutions, forming larger amounts of formate, increases the reducing power allowing the incorporation of larger amounts of Ru in Pt–Ru materials.

A study of the hydrogen oxidation reaction on Pt–Ru materials shows that even with a high Ru contents the mechanism of the reaction is a reversible direct discharge.

The oxidation of CO shows that the onset potential of the reaction clearly decreases when the amount of Ru increases. The reaction is irreversible, with high values of Tafel slope that were interpreted on the basis of the contribution of the two metals to form the reagents.

References

[1] V.C.H.K. Kordesch, G. Simader, Fuel cells and Their Applications, Weinheim, 1996.
[2] E.A. Ticianelli, G.A. Camara, L.G.R.A. Santos, Quím. Nova. 28 (4) (2005) 664.
[3] E.A. Ticianelli, E.R. Gonzalez, Quím. Nova. 12 (3) (1989) 168.
[4] M.P. Hogarth, G.A. Hards, Platinum Met. Rev. 40 (4) (1996) 150–159.
[5] S. Gilman, J. Phys. Chem. 68 (1) (1964) 70.
[6] X. Gang, L. Qingfeng, H. Aage, N. Djerrum, J. Electrochem. Soc. 142 (9) (1995) 2890–2893.
[7] H.A. Gasteiger, N.M. Markovic, N.P. Ross Jr., E.J. Cairns, J. Phys. Chem. 98 (1994) 617–625.
[8] H.A. Gasteiger, N.M. Markovic, N.P. Ross Jr., J. Phys. Chem. 99 (1995) 8290–8301.
[9] H.A. Gasteiger, N.M. Markovic, N.P. Ross Jr., J. Phys. Chem. 99 (1995) 16757–16767.
[10] S. Mukerjee, J. McBreen, J. Electrochem. Soc. 143 (7) (1996) 2285–2294.
[11] W.T. Napporn, J.M. Léger, C. Lamy, J. Electroanal. Chem. 408 (1996) 141–147.
[12] E.M. Crabb, R. Marshall, D. Thompsett, J. Electrochem. Soc. 147 (12) (2000) 4440–4447.
[13] R. Ianniello, V.M. Schmidt, U. Stimming, J. Stumper, A. Wallau, Electrochim. Acta 39 (11/12) (1994) 1863–1869.
[14] N.B. Grgur, N.M. Markovic, P.N. Ross, Eletrochim. Acta 43 (24) (1998) 3631–3635.
[15] D.C. Papageorgopoulos, M. Keijzer, F.A. De Bruijn, Eletrochim. Acta 48 (2002) 197–204.
[16] Z. Hou, B. Yi, H. Yu, Z. Lin, H. Zhang, J. Power Sources 123 (2003) 116–125.
[17] M.P. Hougarth, T.R. Ralph, Platinum Met. Rev. 46 (4) (2002) 146–164.
[18] H. Igarashi, T. Fujino, Y. Zhu, H. Uchida, M. Watanabe, Phys. Chem. Chem. Phys. 3 (2001) 306–314.
[19] F. Colmati Jr., W.H. Lizcano-Valbuena, G.A. Camara, E.A. Ticianelli, E.R. Gonzalez, J. Braz. Chem. Soc. 13 (4) (2002) 474–482.
[20] S. Motoo, T. Okada, J. Electroanal. Chem. 157 (1983) 139.
[21] M. Watanabe, M. Shibata, S. Motoo, J. Electroanal. Chem. 187 (1985) 161.
[22] E.A. Batista, T. Iwasita, W. Vielstich, J. Phys. Chem. B 108 (2004) 14216–14222.
[23] E.R. Gonzalez, E.A. Ticianelli, A.L.N. Pinheiro, J. Perez Patente Brás. INPI-SP no. 00321, 1997.
[24] F. Colmati, V.A. Paganin, E.R. Gonzalez, Simpósio Brasileiro de Eletroquímica e Eletroanalítica SIBEE, 2004.
[25] J.R.C. Salgado, E.R. Gonzalez, Eclética Química 28 (2) (2003) 77.
[26] M. Pourbaix, J.A. Franklin, Atlas of Electrochemical Equilibria in Aqueous Solutions, vol. 348, National Association of Corrosion Engineers, Houston, 1974.
[27] A.J. Bard, R. Parsons, J. Jordan, Standard Potentials in Aqueous Solutions, Marcel Dekker, Inc., New York, 1985, pp. 189–200.
[28] T.J. Schmidt, H.A. Gasteiger, G.D. Stäb, P.M. Urban, D.M. Kolb, R.J. Behm, J. Eletrochem. Soc. 145 (7) (1998) 2354.
[29] A. Essalik, K. Amouzegar, O. Savadogo, J. Appl. Electrochem. 25 (1995) 404.
[30] M. Watanabe, M. Tomikawa, O.S. Motoo, J. Electroanal. Chem. 195 (1985) 81–93.
[31] M. Watanabe, K.K. Makita, H. Usani, O.S. Motoo, J. Electroanal. Chem. 197 (1986) 195.
[32] E.A. Seddon, K.R. Seddon, The Chemistry of Rutenium, Elsevier, New York, 1984.
[33] Z. Hou, B. Yi, H. Yu, Z. Lin, H. Zhang, J. Power Sources 123 (2003) 116.
[34] C. Giacovazzo, H.L. Monaco, D. Viterbo, F. Scordari, G. Gilli, G. Zanotti, M. Catti, Fundamentals of Crystallography, vol. 154, Oxford Science Publications, 1992.
[35] International tables for X-ray crystallography, The International Union of Crystallography, D. Reidel Publishing Company, Boston, 1985.
[36] S. Enbäck, G. Lindberg, J. Eletrochem. Soc. 152 (1) (2005) A23–A31.
[37] M. Watanabe, S. Motoo, J. Electroanal. Chem. 382 (1995) 65.
[38] A.M.C. Luna, G.A. Camara, V.A. Paganin, E.A. Ticianelli, E.R. Gonzalez, Eletrochem. Commun. 2 (2000) 222.
[39] F.H.B. Lima, M.J. Giz, E.A. Ticianelli, J. Braz. Chem. Soc. 16 (3A) (2005) 328–336.
[40] M.W. Breiter, Electrochemical Processes in Fuel Cells, Springer, Berlin, 1969.
[41] B.E. Conway, Theory and Principles of Electrode Processes, The Ronald Press Company, New York, 1965.

[42] J.A. Harrison, Z.A. Khan, J. Electroanal. Chem. 30 (1971) 327.
[43] H.J. Flitt, J.O'm. Bockris, Int. J. Hydrogen Energy 7 (1982) 411.
[44] A.S. Arico, E. Modica, E. Passalacqua, V. Antonucci, P.L. Antonucci, J. Appl. Electrochem. 27 (1997) 1275.
[45] A.S. Arico, E. Modica, P. Creti, P.L. Antonucci, V. Antonucci, J. New Mater. Electrochem. Syst. 3 (2000) 207.
[46] D. Aberdam, R. Durand, R. Faure, F. Gloaguen, J.L. Hasemann, E. Herrero, A. Kabbabi, O. Ulrich, J. Electroanal. Chem. 398 (1995) 43.
[47] G.A. Camara, E.A. Ticianelli, S. Mukerjee, S.J. Lee, S.J. Mcbreen, J. Eletrochem. Soc. 149 (6) (2002) 748.
[48] J.O'm. Bockris, S.U.M. Khan, Surface Electrochemistry, Plenum Press, New York, 1993, p. 277.